Engineering Structures 300 (2024) 117141

Contents lists available at ScienceDirect

Engineering Structures

journal homepage: www.elsevier.com/locate/engstruct

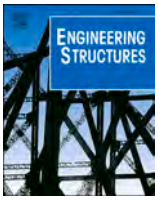

Blended structural optimization of steel joints for Wire-and-Arc Additive Manufacturing

Vittoria Laghi [a,*], Neira Babovic [b], Edoardo Benvenuti [a], Harald Kloft [b]

[a] Department of Civil, Chemical, Environmental and Materials Engineering (DICAM) - University of Bologna, Bologna, Italy
[b] Institute of Structural Design (ITE) – Technische Universität Braunschweig, Braunschweig, Germany

ARTICLE INFO

Keywords:
Directed energy deposition
Topology optimization
Steel structures
Joint classification

ABSTRACT

Metal Additive Manufacturing, and in particular Wire-and-Arc Additive Manufacturing (WAAM) has proved to be a great and efficient alternative to the common subtractive manufacturing processes to realize complex-shape members and connections for construction. With reference to complex spatial structures such as gridshells, the connections play a crucial role both in the design and the construction processes. Novel computational design tools allow designers to conceive optimized joint solutions while minimizing the material use, resulting in difficult geometries to be fabricated with conventional methods. The present work aims at providing an innovative integrated design and fabrication framework to efficiently apply topology optimization algorithms to improve the efficiency of steel joints in complex spatial structures. The framework is based on the so-called "blended" structural optimization approach aimed at incorporating manufacturing constraints, basic principles of conceptual structural design and structural requirements into topology optimization to design ready-to-fabricate complex steel joints. The designs are suitable for fabrication with the WAAM process. The approach is applied to a case study to re-design the joint connections of the world's renowned British Museum gridshell rooftop structure. From a catalogue of various designs for each unique joint, one selected design is optimized and then checked for structural requirements in terms of strengths and stiffness. Then the optimized joint is validated for fabrication with WAAM process.

1. Introduction

The adoption of digital solutions for construction has proved to increase work safety and support the Circular Economy, by reducing the material waste and simplifying the resource recapture [1,2]. Additive Manufacturing (AM, or 3D printing) processes have the great advantage of flexibility in the geometry of the outcome. This aspect appears to be most suitable for the realization of efficient forms which are difficult to realize with conventional manufacturing techniques but result in a severe reduction in the material use. Such forms could be achieved with the use of novel Algorithm-Aided Design (AAD) [3] tools, already commonly used in other industrial sectors, such as automotive and aerospace.

The application of both AM solutions and computational design tools for steel structures have always been limited to few pioneering cases. Recent developments of AM process in construction have seen the application of these techniques to realize a new generation of structures in concrete, polymers and metals [4,5]. Regarding applications in steel structures, the most developed metal AM technology (Powder-Bed Fusion, PBF) has often limited the maximum dimension of the printed outcomes. Thus, it has been adopted to realize ad-hoc connections parametrically designed either for structural optimization purposes [6] or to create free-form gridshells [7]. However, due to the intrinsic geometrical constraints of the printer environment (enclosed in a box of typically 250-mm size), the application of PBF process is limited to the realization of small-size connections and structural details [8]. More recently, Directed-Energy Deposition (DED) techniques such as Wire-and-Arc Additive Manufacturing (WAAM) allowed to increase the dimension of the printed outcomes up to several meters of span, thus increasing the potential use of digital fabrication in steel construction [9]. The first application of this technique is the MX3D Bridge, the world's first steel 3D printed footbridge, currently located in Amsterdam city centre [10]. Another example on the application of structural optimization and WAAM technique has been proposed by a research group from TU Delft. The Glass Swing has been realized in structural glass and WAAM-produced steel joints by the Dutch company RAMLAB

* Corresponding author.
E-mail address: vittoria.laghi2@unibo.it (V. Laghi).

https://doi.org/10.1016/j.engstruct.2023.117141
Received 27 February 2023; Received in revised form 22 August 2023; Accepted 6 November 2023
Available online 20 November 2023

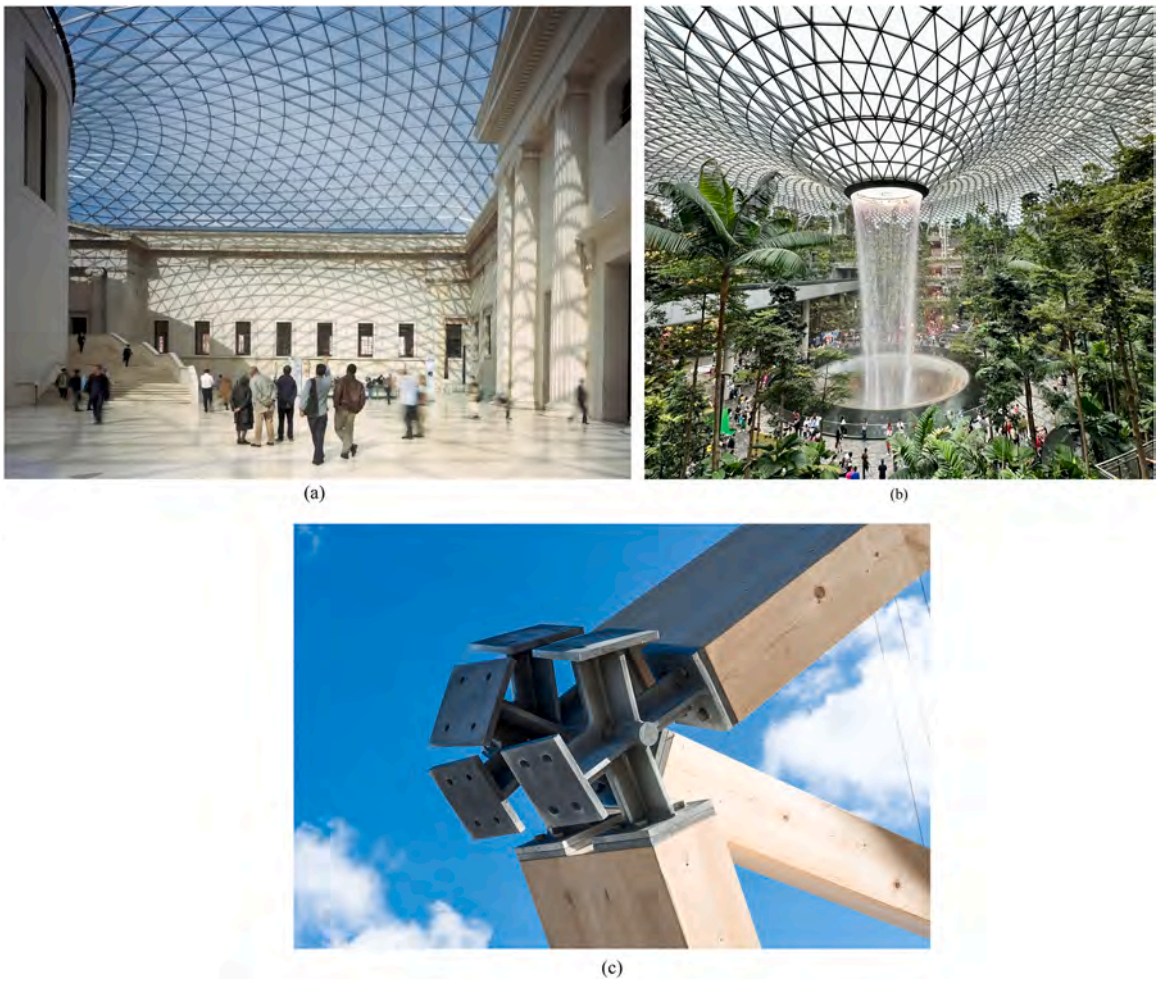

Fig. 1. Example of complex spatial structures: (a) British Museum rooftop (credits: Foster+Partners); (b) Changi Airport (credits: Vittoria Laghi); (c) Canary Wharf crossrail roof (credits: Foster+Partners).

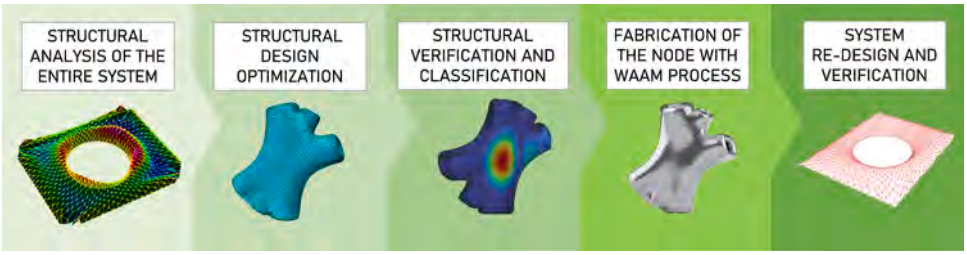

Fig. 2. Graphical representation of the "blended" optimization workflow.

[12]. The non-standard form of the swing was developed through ad-hoc optimization procedure for vector active glass structures [13]. Very recently, the research group from TU Darmstadt presented the potentials of production and post-processing of steel joint connections realized in WAAM [14].

The computational design freedom of creating new structural forms was limited to the traditional building production which does not allow for such freedom. Hence, the application of computational design tools for free-form design was often limited to few explorations in pioneering architectural applications. With the advent of AM process in construction, the use of structural optimization could potentially allow to realize a new generation of optimized structures [15]. Current research effort is paid to combine AM with optimization tools to solve issues related to manufacturing processes (such as overhang, see e.g.[16]) or exploit the material anisotropy to find new optimal solutions (see e.g. [17,18]).

2. Problem formulation

Lightweight steel structures such as gridshells, truss systems and spatial structures have the great advantage of minimizing the weight while guaranteeing good structural performances in terms of stiffness and strength. Over the last two decades great effort has been made to realize more complex spatial structures (usually in steel or wood) fully exploiting the novel computational design tools toward high-end architectural buildings [19–21]. Examples of complex spatial structures, such as gridshell roofs, are, among others: the BMW Pavillion for the 1999 Expo [22], the British Museum gridshell [19], the "Bird's nest" Beijing stadium [23], the Singapore Changi Airport Jewel rooftop [24],

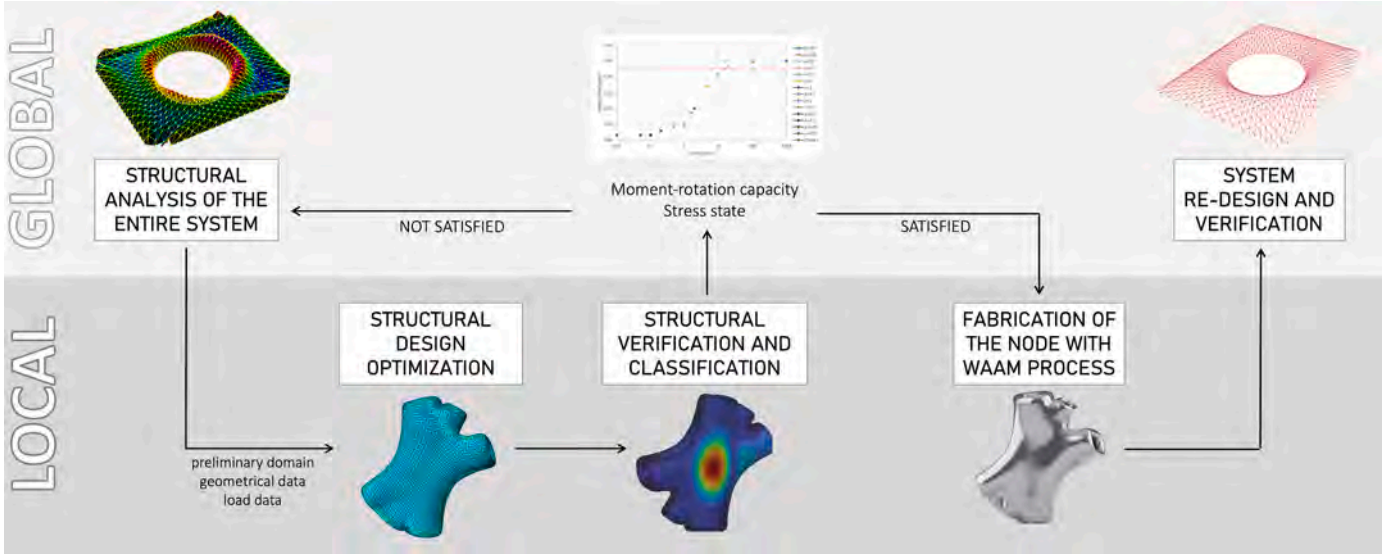

Fig. 3. Workflow: global-local interaction.

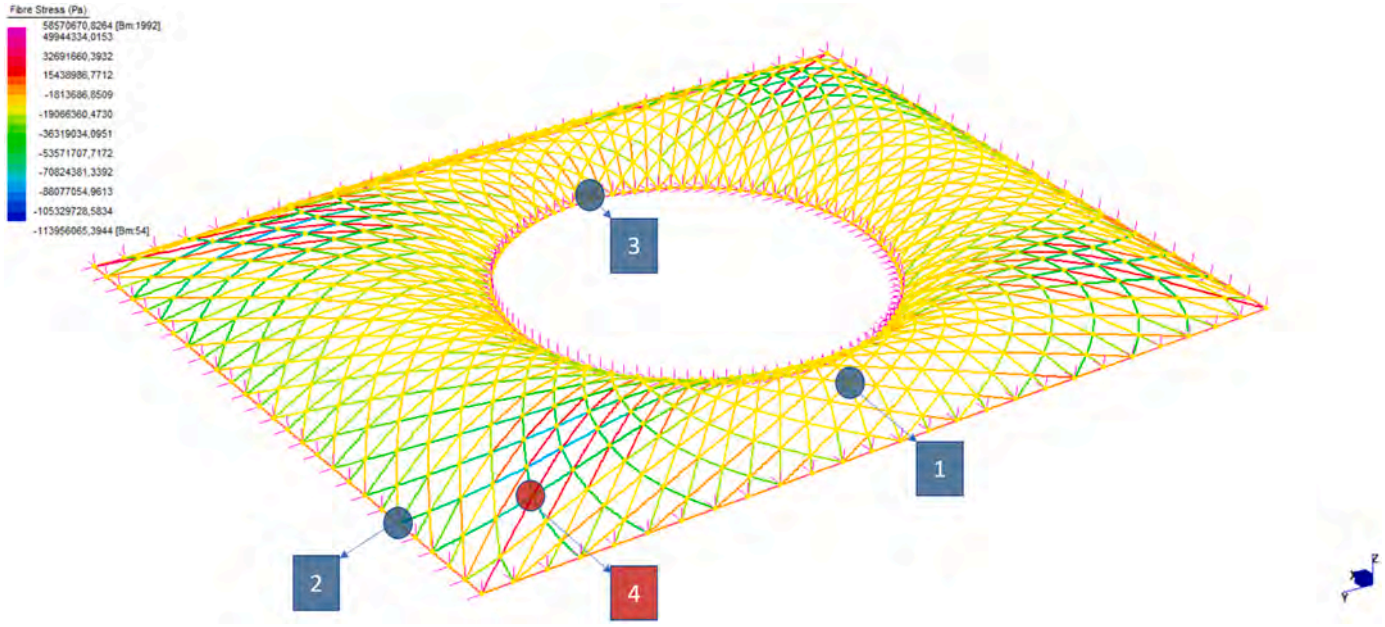

Fig. 4. Structural analysis of the gridshell with selected characteristic joints.

the Dutch Maritime Museum gridshell roof [19], the Canary Wharf crossrail station designed by Foster+Partners [25] (Fig. 1).

Although their high aesthetic and structural performances, the critical issue of all these complex structures lie in the connection of each individual element. Complex welding, CNC and cast iron are the most commonly adopted techniques to fabricate these spatial joints. Hundreds of unique joints were fabricated with CNC machine for the realization of the British Museum gridshell, resulting in huge material waste and large production time [26]. Complex welding was adopted to realize over 500 individual spatial joints for the rooftop of the Canary Wharf wooden gridshell, resulting in increase in time to finalize the structure [25].

Over the last years AM techniques combined with topology optimization tools have been exploited to suggest new spatial steel joints for complex structures. Indeed, the flexibility of AM process in creating various geometrical shapes has been used to realize new types of joints for steel structures, with the aim of reducing the complexity of the construction of truss systems. The first example was the topology optimized joint conceived by Arup and fabricated with PBF [27]. Another example was proposed by MX3D in collaboration with Takenaka producing a composite concrete and steel joint whose external skin was fabricated with WAAM [11]. Kanyilmaz et al. [28] recently proposed bamboo-inspired optimized steel tubular joints. Wang et al. [29] developed an integrated method to design joints for tree-like structures.

Among various metal AM processes, Wire-and-Arc Additive Manufacturing (WAAM) has resulted the most suitable to realize structural elements and joints, for the high production flexibility in geometry and size while maintaining good mechanical properties. However, specific considerations must be made when dealing with the structural performances of WAAM elements: (i) the inherent surface roughness [30], (ii) the marked mechanical anisotropy [31–33], (iii) the influence of process parameters [34]. The calibration of the printing parameters in the fabrication process severely alters the mechanical and geometrical features of the structural element. WAAM structures require a

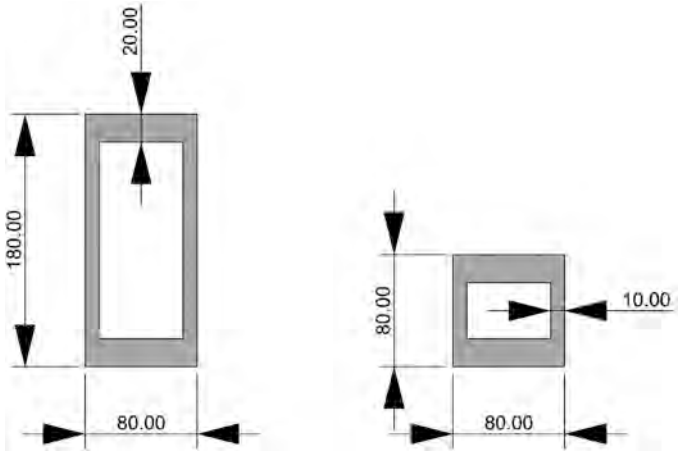

Fig. 5. Cross-section dimensions from literature (members near quadrangle – left, members near center/reading room – right).

force-flow-oriented architectural and structural design. In particular, manufacturing constraints and limitations require new methods for the selection of design techniques. Additionally, anisotropic mechanical properties need to be taken into account during the design phase to engineer the material according to the printing direction.

For this aim, an integrated design and fabrication framework is here proposed (Section 3) in the form of "blended" structural optimization as first conceived for the realization of WAAM-produced optimized beams (see e.g. [35]).

3. "Blended" structural optimization approach for WAAM steel joints

The present work aims at solving the current issue in the design and fabrication of steel connections for complex spatial structures by integrating novel computational design algorithms with digital fabrication.

The workflow is based on the so-called "blended" optimization approach recently proposed by [35]. This integrated design framework is proposed to be adaptive with respect to different structural applications and printing strategies and capable of accounting not only for the process constraints but also the anisotropic feature of the printed alloys. This way, the outcome will be able to efficiently use the material

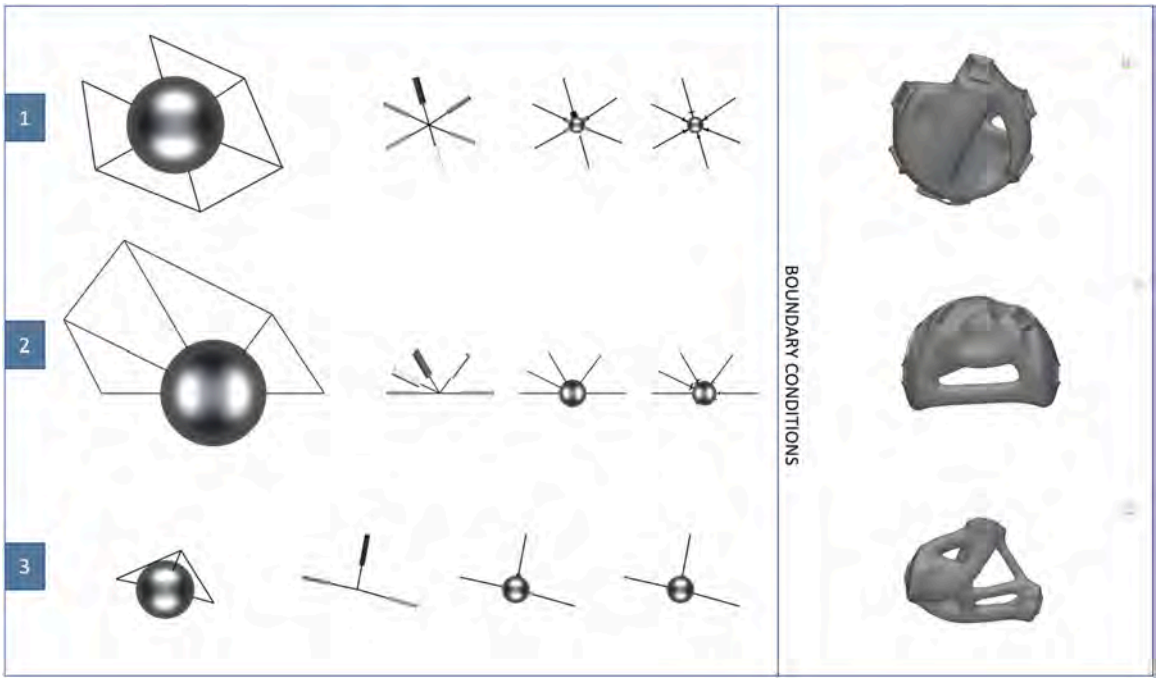

Fig. 6. Initial spherical domain for three selected joints, with the corresponding members and resulting topologies.

Fig. 7. Initial domain and members of the critical joint with its final topology.

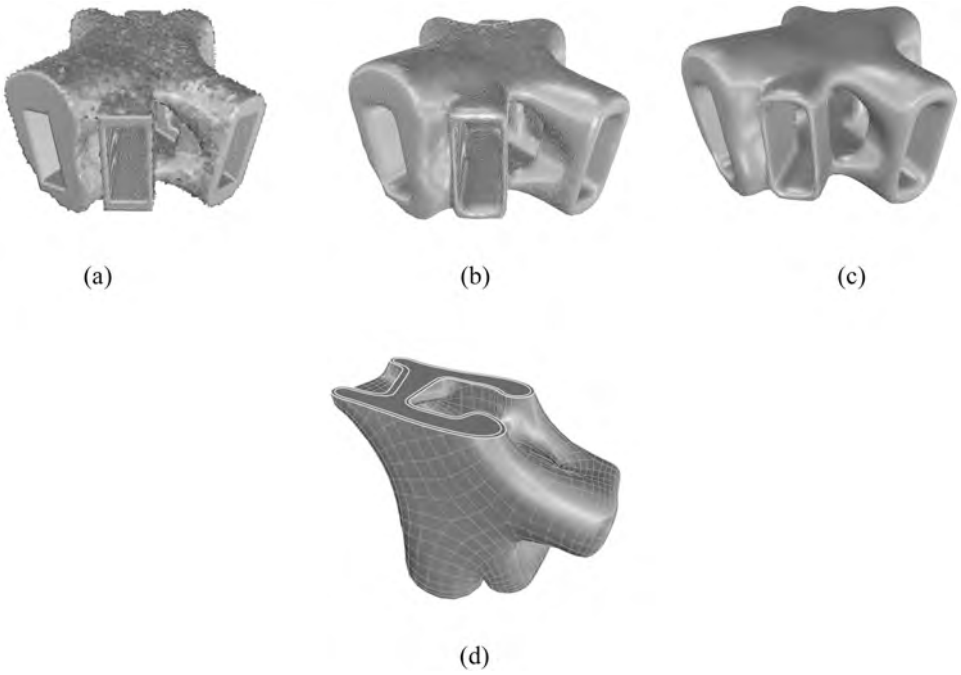

Fig. 8. (a),(b),(c) sequential optimization phases; (d) final 6 mm-shell joint element.

Table 1
Buckling factors and loads for 6-mm thickness joint.

	Beam01	Beam02	Beam03	Beam04	Beam05	Beam06
	Buckling factors					
Mode 1	19.1431	20.6393	29.533	22.8698	28.1665	23.5258
Mode 2	22.1683	21.4959	34.9671	24.3694	31.3702	26.9124
Mode 3	23.4929	29.2497	38.014	33.9301	33.0674	27.686
Mode 4	27.1755	31.0123	38.1241	37.9618	33.9804	28.548
	Buckling loads (kN)					
Mode 1	19143.1	20639.3	29533	22869.8	28166.5	23525.8
Mode 2	22168.3	21495.9	34967.1	24369.4	31370.2	26912.4
Mode 3	23492.9	29249.7	38014	33930.1	33067.4	27686
Mode 4	27175.5	31012.3	38124.1	37961.8	33980.4	28548

properties and accommodate different structural outcomes and real-case scenarios for future use in the construction industry. The framework is based on mechanical and manufacturing constraints proper of a metal AM technique particularly suitable for construction structural applications, i.e. Wire-and-Arc Additive Manufacturing (WAAM).

The design of steel connections is developed considering the structural analysis of the global structure, by integrating basic principles of structural design with topology optimization algorithms. A catalogue of possible solutions is then checked for the structural requirements in terms of strengths and stiffness. Both the designs and the verifications account for the possible anisotropic behavior of the printed outcomes realized with WAAM. In fact, recent studies demonstrated that WAAM-produced alloys present a non-negligible anisotropic response both in the elastic and post-elastic field. Finally, the selected designs are adapted considering the manufacturing constraints proper of the selected printing process. The newly designed connections are then embedded into the global structure and validated. A graphical representation of the workflow is depicted in Fig. 2.

The proposed workflow is adapted to consider both the global (i.e. the whole structure) and the local (i.e. the single connections) scale. At the global scale, the entire system is analyzed and eventually re-designed according to the specific considerations collected for the joints. At the local scale, the attention is focused on the joint optimization and stiffness classification, which governs the overall structural behavior and also the configuration of the whole system (e.g. in terms of members size). This global-local interaction is depicted in Fig. 3.

3.1. Structural design optimization

Within the framework of the blended optimization approach, the first step is the definition of a catalogue of possible designs developed through topology optimization algorithms. For the structural design optimization of the joints, a stiffness-based topology optimization is adopted. The designs are developed considering basic principles of structural design, together with concepts of robustness and reliability to guide the designer from purely mathematically-optimized solutions towards a structural-consistent design. For this aim, various boundary and loading conditions are used to conceive a catalogue of possible solutions from which the designer can attain from. A preliminary check of the structural performances of the designs is also carried out through the algorithm.

3.2. Structural verification and stiffness classification

Once the possible designs are catalogued, advanced analysis of the structural performances in terms of strengths and stiffness is performed. In detail, the selected designs are checked for the structural strengths under tensile and compressive loading conditions, with specific attention to possible local buckling failures. For this aim, Finite Element Analysis is carried out. The analysis is developed to account for the possible anisotropic behaviour of the printed elements.

A further step in the verification process is the evaluation of the joint stiffness. This aspect is particularly important in complex spatial structures as the different level of stiffness of the joint would alter the whole design conception of the global structure. For this aim, Eurocode 3 Part 1–8 classifies joints into three different categories according to their stiffness and their strength capacity [36]. Regarding stiffness classification, the categories are:

- Nominally pinned joints: they should be capable of transmitting the internal forces, without developing significant moments which might adversely affect the members or the structure as a whole, and should be able of accepting the resulting rotation under the design loads;

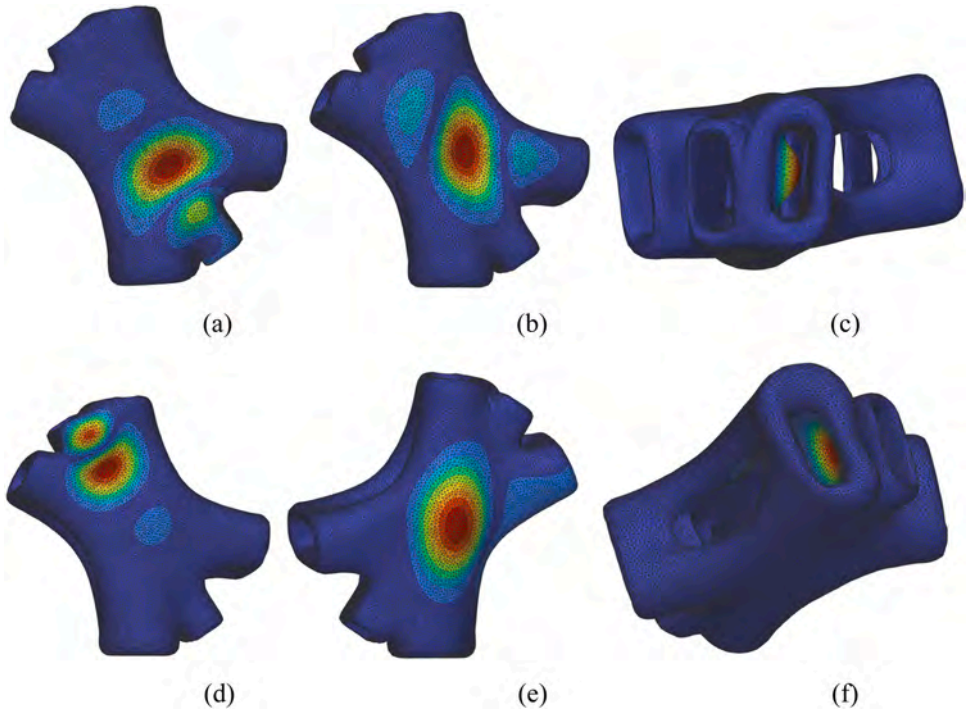

Fig. 9. Deformed shapes for mode 1 considering the joint with a thickness of 6 mm: (a) Beam 01, (b) Beam 02, (c) Beam 03, (d) Beam 04, (e) Beam 05, (f) Beam 06.

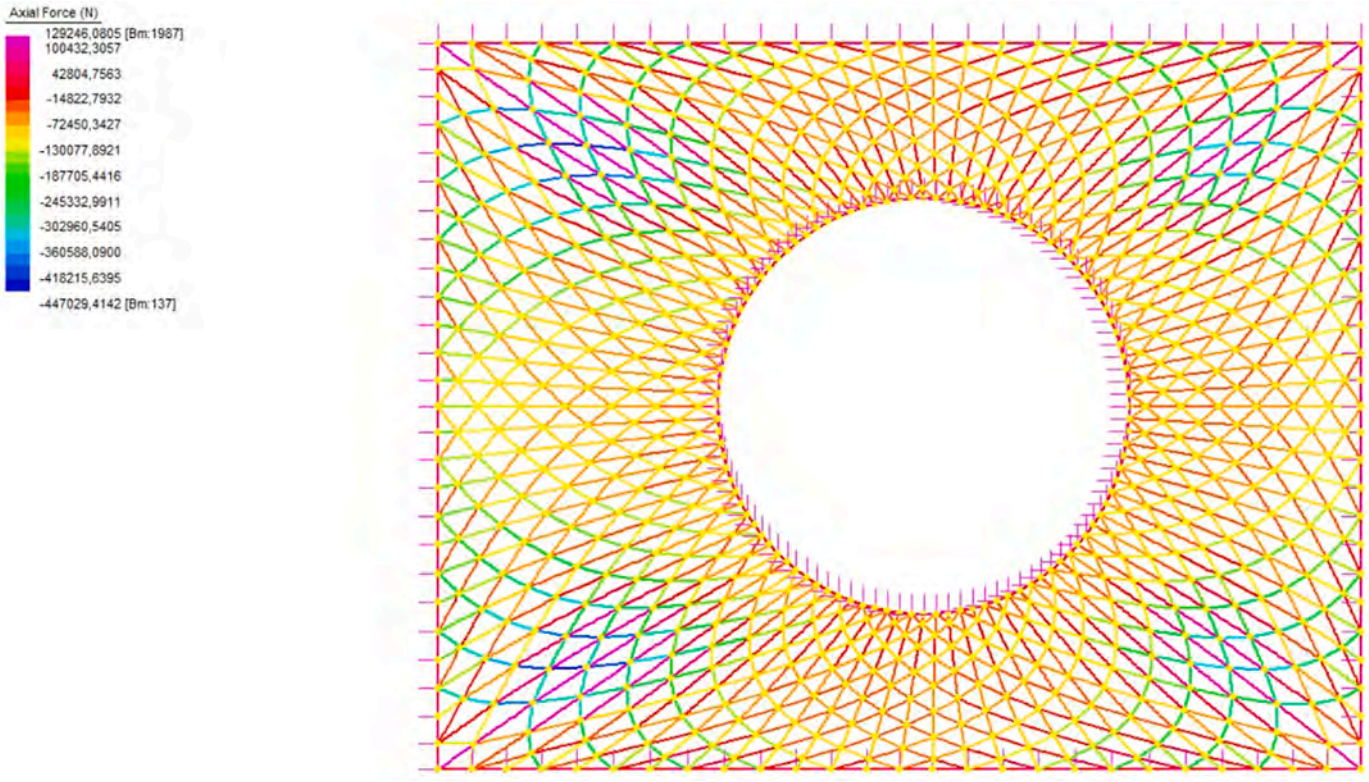

Fig. 10. Axial force distribution in the gridshell.

- Rigid joints: they may be assumed to have sufficient rotational stiffness to justify analysis based on full continuity;
- Semi-rigid joints: they do not meet the criteria for rigid joints or nominally pinned joints and they should be capable of transmitting the internal forces and moments.

Regarding strength classification, the categories are:

- Nominally pinned joints: they should be capable of transmitting the internal forces, without developing significant moments which might adversely affect the members or the structure as a whole;
- Full strength joints: the design resistance should be not less than that of the connected members;

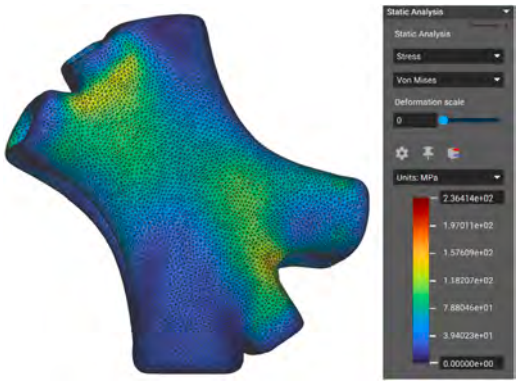

Fig. 11. Stress distribution considering the joint.

Table 2
Computation of λ for different values of α.

α	K_{11} (Nm)	K_{22} (Nm)	K_{33} (Nm)	Load Increment	λ
Pinned	0	0	0	0.18	0.06
0.01	14713	3018	2687	0.18	0.06
0.05	73567	15088	13435	0.18	0.06
0.10	147135	30175	26871	0.19	0.06
0.20	294269	60351	53741	0.35	0.11
0.50	735673	150877	134353	0.53	0.17
1	1471345	301754	268707	0.60	0.20
1.50	2207018	452632	403060	1.05	0.34
2	2942690	603509	537413	1.23	0.40
5	7356725	1508772	1343534	2.08	0.67
10	14713450	3017544	2687067	2.55	0.83
15	22070175	4526316	4030601	2.75	0.90
20	29426901	6035088	5374134	2.86	0.93
100	147134503	30175439	26870670	3.03	0.98
Rigid	∞	∞	∞	3.08	1.00

- Partial-strength joints: they do not meet the criteria for full-strength joints or nominally pinned joints.

Recent research work carried out by Fan et al. [37] described a simplified method to analyze the joint behavior based on the Eurocode provisions. In particular, the classification of the joints is based on both stiffness and strength criteria as follows:

- Rigid joints: they have high rotational strength and high rotational stiffness;
- Pinned joints: they have low rotational strength and low rotational stiffness;
- Semi-rigid joints: they have moderate rotational strength and moderate rotational stiffness.

The procedure is based upon the moment capacity of the joints, from which two coefficients α and β are determined on stiffness and strength considerations, respectively. Details on the numerical procedure can be found in [37]. Combining the results obtained in terms of stiffness and strength, the joints can be classified as rigid, semi-rigid and pinned based on the respective values of α and β.

3.3. WAAM fabrication process

The final step before implementing the optimized designs into the global structure is the fabrication of the joints. A feasibility study is carried out to ensure that the proposed design responds to the manufacturing constraints proper of the selected printing process, i.e. WAAM. The main fabrication issues are: overhang, deformations due to heat accumulation and over-deposition of the material at start-and-stop points. Commercially-available software tools allow to simulate the fabrication steps and define the path planning accordingly. In this final step the design could undergo some adjustments to facilitate the fabrication process.

4. Case study of an optimized WAAM joint for the British Museum

4.1. Structural analysis of the British Museum gridshell

The British Museum was constructed in the 18th century and it is arranged as a quadrangle surrounding the Great Court, the centerpiece of which is the historic Reading Room. Initially, the Great Court was occupied by the British Library but now it has been transformed into an elegant public space covered by a glazed roof the size of a football field. This new space allowed to design new galleries and a destination restaurant. The erection of the glazed roof began in 1999, it has been completed and opened to the public in November 2000.

The structural analysis of the gridshell roof has been carried out on a model realized with the parametric software Grasshopper, simulating the form-finding procedure from 1999. Starting from the initial boundaries of the roof, the initial plane surface has been generated and subsequently meshed. Its joints and edges have been used to obtain the curved surface of the British Museum, applying some forces, boundary conditions and stiffnesses to the members. Finally, the grid has been drawn on the previously derived surface. The gridshell structure has been structurally analyzed using Straus7 software to extract the stresses acting on each joint.

Afterwards, these stresses will be useful to perform the topology optimization of one joint in order to study its strength and stiffness. The interaction between global – structural system (e.g. gridshell) and local – structural connection (e.g. WAAM joint) is presented as a loop design procedure, as proposed in Fig. 3.

The chosen joint has been selected for its critical location (location

Table 3
Computation of λ for different values of β.

Computation of λ for different values of β with an initial α							
β	*α*	$M_{pl,plane_1}$ (Nm)	$\chi_{pl,plane_1}$ (1/m)	$M_{pl,plane_2}$ (Nm)	$\chi_{pl,plane_2}$ (1/m)	*Load Increment*	λ
0.01	20	458	0.000444	992	0.000197	0,15	0,05
0.02	20	916	0.000888	1985	0.000394	0.30	0.11
0.05	20	2290	0.002219	4962	0.000986	0.65	0.23
0.08	20	3664	0.003550	7939	0.001578	1.01	0.36
0.10	20	4580	0.004438	9924	0.001972	1.19	0.42
0.20	20	9159	0.008875	19848	0.003944	1.84	0.64
0.30	20	13739	0.013313	29773	0.005917	2.24	0.79
0.40	20	18318	0.017750	39697	0.007889	2.53	0.89
0.50	20	22898	0.022188	49621	0.009861	2.68	0.94
0.80	20	36636	0.035500	79394	0.015778	2.84	1.00
1	20	45795	0.044375	99242	0.019722	2.85	1.00
Rigid	20	∞	∞	∞	∞	2.85	1.00

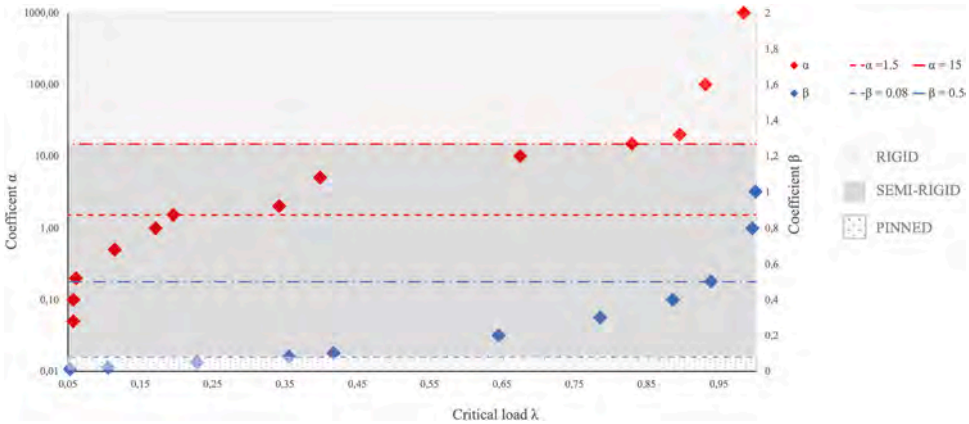

Fig. 12. Combined α and β plot for joint classification.

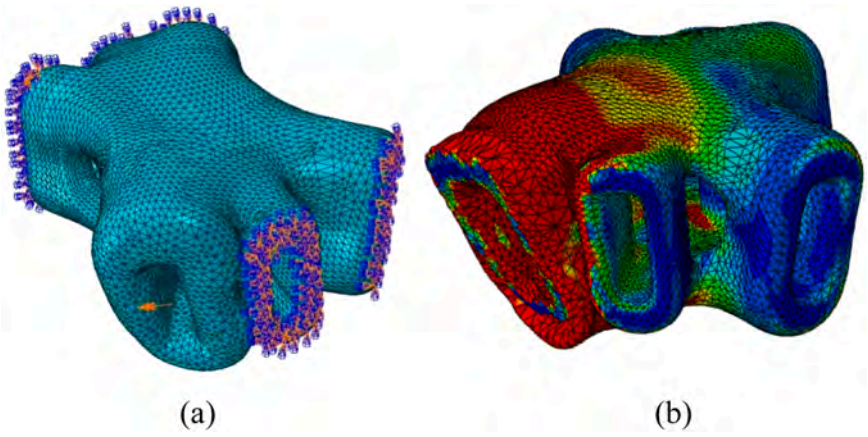

Fig. 13. (a) Example of loads and boundary conditions; (b) example of stress distribution and joint deformation.

Table 4
Joint classification for 6-mm thickness joint and moments in X-X direction.

Directions		k_j(kNm/rad)	k_b(kNm/rad)	M_j(*kNm*)	M_b(*kNm*)	α	β	Verification
01	M +	10554.57	1471.35	62.55	99.24	7.17	0.63	Semi-Rigid
	M −	10563.41		62.31		7.18	0.63	Semi-Rigid
02	M +	9529.80	1471.35	69.75	99.24	6.48	0.70	Semi-Rigid
	M −	9525.59		70.35		6.47	0.71	Semi-Rigid
03	M +	18260.29	1471.35	72.33	99.24	12.41	0.73	Semi-Rigid
	M −	18231.62		74.55		12.39	0.75	Semi-Rigid
04	M +	13520.36	1471.35	64.40	99.24	9.19	0.65	Semi-Rigid
	M −	13501.58		65.16		9.18	0.66	Semi-Rigid
05	M +	11948.27	1471.35	72.03	99.24	8.12	0.73	Semi-Rigid
	M −	11945.78		72.86		8.12	0.73	Semi-Rigid
06	M +	15453.97	1471.35	71.75	99.24	10.50	0.72	Semi-Rigid
	M −	15458.95		77.22		10.51	0.78	Semi-Rigid

number 4 in Fig. 4), where the maximum stresses and strains are present. Once the joint of the British Museum has been chosen to optimize, the initial domain, loads, boundary conditions and constraints of this structural joint are defined to perform the topology optimization.

4.2. Structural design optimization of the characteristic joints

Fig. 4 shows each joint's unique loading and geometrical configuration and consequential requirement for their individual assessment. This can be simplified with the axes of symmetry and patterns present in the gridshells, where a certain level of repetitiveness is expected, for example, the number of members at a joint (Fig. 5). Clustering the joints based on their position in the gridshell, the number of intersecting beams or inclination can streamline the analysis. The following characteristic locations are selected to determine the expected topology of the joints:

1. Central, six-member joint at inflection point of the curve (angle of the joint ~ 0°)
2. Edge, five-member joint at the quadrangle edge (inclined)
3. Edge, three-member joint at the reading room edge (inclined)

The joint initial domain for the optimization analysis is defined with spherical geometry to provide significant space for the joint to be shaped, and the size (the diameter of the sphere) is determined such that it avoids the intersection of adjacent members outside of the joint.

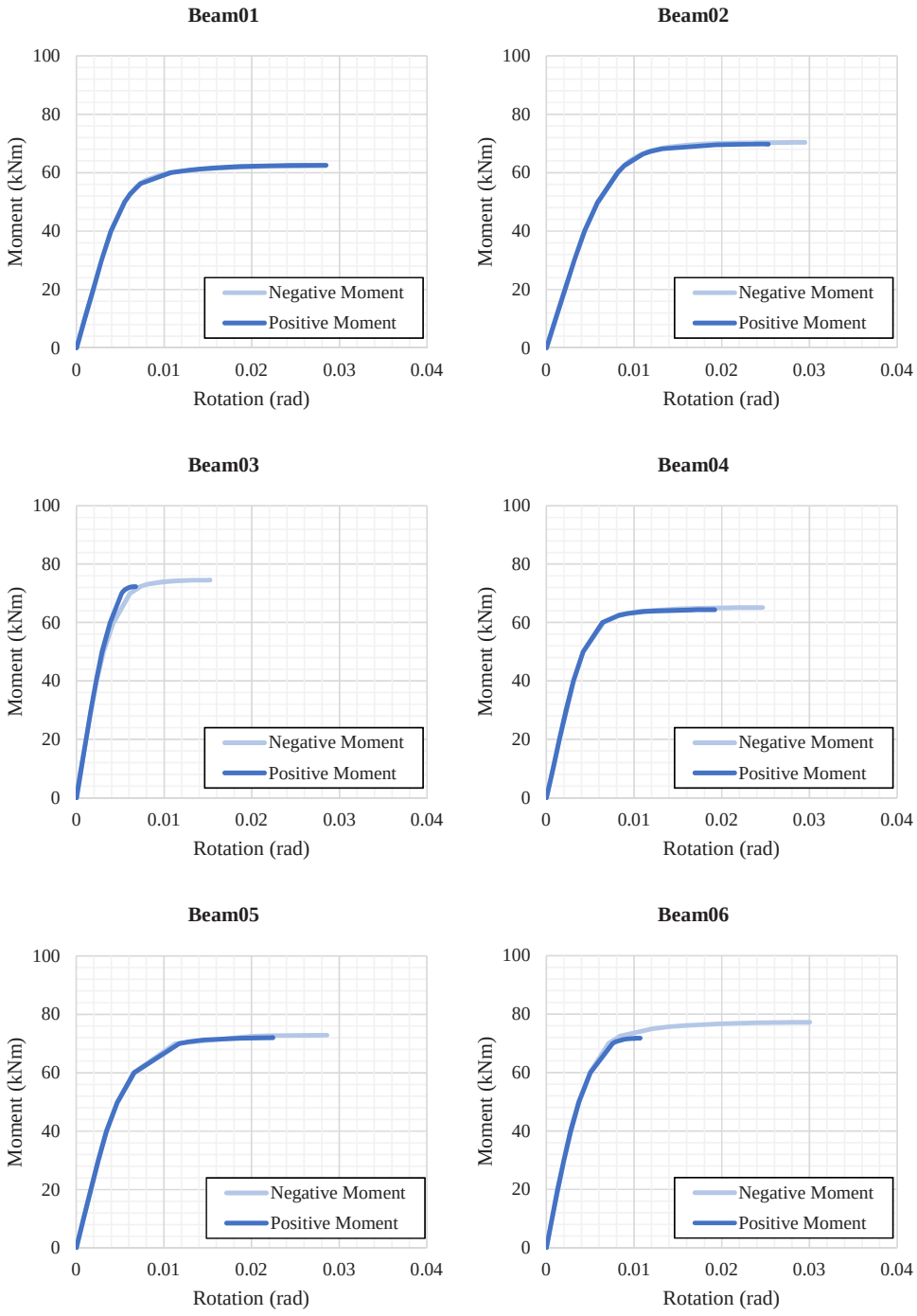

Fig. 14. Moment-rotation graphs considering a 6 mm thickness joint and moments in X-X direction.

Therefore, depending on the angle between the members, as well as the inclination of the joint, initial domains (spheres) have different diameters, which consequently result in joints of different sizes (Fig. 6).

Once the initial domain has been created, loads and boundary conditions are to be set. Displacement boundary conditions (i.e., supports) have been applied only on one profile, which is considered clamped. The proposed boundary condition definition is partially based on the support requirements during the fabrication phase and therefore helps to maintain the assumption of a self-supporting geometry (prior to overhang evaluation). This deviation from the Straus7 boundary condition definition is compensated through redistribution of the load of the profile restrained on the other members. Loads have been applied considering the stresses obtained from Straus7.

4.2.1. *Boundary conditions and an initial domain*

In order to properly connect the beams to the joint, it is mandatory to define some regions that will not be included in the optimization process. In correspondence to the six profiles and internally to the initial domain, non-design domain of 10-cm length has been created and excluded from the topology optimization analysis (Fig. 7 - red).

4.2.2. *Topology optimization*

The selected joint is optimized considering the following geometrical requirements: the holes must be distributed inside the final geometry of the joint, the holes in correspondence of the beams do not have to present any type of additional opening and the remaining material must be distributed almost uniformly.

Table 5
Joint classification for 6-mm thickness joint and moments in Y-Y direction.

Directions		k_j(kNm/rad)	k_b(kNm/rad)	$M_j(kNm)$	$M_b(kNm)$	α	β	Verification
01	M +	3138.75	301.75	29.35	45.80	10.40	0.64	Semi-Rigid
	M −	3125.43		28.89		10.36	0.63	Semi-Rigid
02	M +	4663.03	301.75	42.16	45.80	15.45	0.92	Rigid
	M −	4670.55		42.26		15.48	0.92	Rigid
03	M +	8042.21	301.75	36.66	45.80	26.65	0.80	Rigid
	M −	8030.16		37.15		26.61	0.81	Rigid
04	M +	4420.63	301.75	31.01	45.80	14.65	0.68	Semi-Rigid
	M −	4402.19		29.24		14.59	0.64	Semi-Rigid
05	M +	4136.54	301.75	37.55	45.80	13.71	0.82	Semi-Rigid
	M −	4127.92		37.08		13.68	0.81	Semi-Rigid
06	M +	6063.69	301.75	35.90	45.80	20.09	0.78	Rigid
	M −	6069.53		37.96		20.11	0.83	Rigid

In order to satisfy the aforementioned requirements, the optimization analysis was performed using a Bi-Linear Evolutionary Structural Optimization (BESO) within the Ameba plug-in in Grasshopper developed by [38]. The following parameters were set before the optimization: volume target equal to 15% and evolutionary ratio equal to 2%.

From the obtained result, the optimized design was "blended" according to the procedure described in [35] to create a smoother design more suitable for printing (Fig. 5). This included variations of load cases extracted from Straus7, displacement boundary conditions, volume target manipulation and an overall, iterative process to reach the final structurally verifiable and manufacturing-suitable design. Following that was post-processing integrating manufacturing constraints of layer thickness for the definition of the final design as either – volume, thick wall shell (12-mm) or thin wall shell (6-mm). Finally, the geometry was adapted into a 6mm shell from the solid element to save material and therefore also production time and cost (Fig. 8d).

4.3. Structural verification and stiffness

4.3.1. Buckling analysis and stress distribution

Previously referred plug-in, Ameba, allows for preliminary structural verification through a display of Von Mises stress, principal stress and deformations. However, geometry then undergoes a post-processing design stage that is characterized by manufacturing constraints, such as layer thickness. Therefore, the final verification needs to be conducted on the modified geometry, in this case – 6-mm shell, (see Fig. 8d). The optimized joint is subjected to compression loads, therefore it is necessary to study the ultimate load before instability phenomena occur. In order to evaluate the ultimate buckling load, the joint has been examined using the "Buckling Analysis" block in nTopology software and studying one profile direction at a time. Then, the buckling analysis determined a "buckling coefficient", which multiplied by the initial load applied allowed to compute the ultimate buckling load. The buckling analysis has been performed on the joint taking into account the 6-mm thickness and the initial compression load applied corresponding to 1000 kN. The results are summarized in Table 1.

The deformed shapes for mode 1, which is the one with the lowest eigenvalue, are reported in Fig. 9.

Comparing the buckling loads with the maximum compression load at the ultimate limit state condition obtained from Straus7, equal to 447 kN (Fig. 10), it can be noted that the design forces used for the optimized joint are well below these limits.

The last verification performed consisted of the assessment of the maximum stress values in the joint at the ultimate limit state. The verification has been carried out using nTopology (Fig. 11). The maximum stress resulted in 236 MPa for the 6-mm thickness joint, which is lower than the yielding limit, therefore the stress verification is satisfied.

4.3.2. Determination of the joint stiffness classification according to Eurocode provisions

In order to study the behaviour of the considered joint, it is necessary to follow these steps:

- Evaluation of the limits of to classify the joint stiffness (Section 4.3.1);
- Evaluation of the limits of to classify the joint strength (Section 4.3.2);
- FEA of the joint to obtain the moment-rotation graph in each direction (Section 4.3.3).

A new coefficient λ that is the ratio of the critical load of the lattice shell with flexible joints $P_{cr,\alpha}$ to that of the rigidly jointed shell $P_{cr,rigid}$ is introduced as follows:

$$\lambda = \frac{P_{cr,\alpha}}{P_{cr,rigid}}$$

The criteria to choose the boundaries for α and β are:

- If the ratio λ is greater than or equal to 90%, the joint will be considered rigid;
- If the ratio λ is smaller than or equal to 30%, the joint will be considered pinned;
- If the ratio λ is between 30% and 90%, the joint will be considered semi-rigid.

The software Straus7 is employed to compute the critical load of the structure. The critical load for the stiffness classification is computed considering the following values of α: Rigid, 100, 20, 15, 10, 5, 2, 1.5, 1, 0.5, 0.2, 0.1, 0.05, 0.01, Pinned. The profiles used in this structure are rectangular hollow cross-sections with the following properties: B= 80 mm, H= 120 mm, t_1= 20 mm, t_2= 10 mm (see Fig. 5). From these, the stiffness of the beam can be calculated along the principal directions (i.e. $R_{11} = \frac{EI_{11}}{L}$, $R_{22} = \frac{EI_{22}}{L}$, $R_{12} = \frac{GJ_T}{L}$). The stiffness in the joint is applied using the command "End Release" in "Beam Attributes" and the values used in the three directions are simply the product of the stiffnesses of the beam for the coefficient α considered.

Before starting the analysis, the nonlinearity of material and section are defined as perfectly elasto-plastic. Based on the aforementioned properties, a non-linear analysis has been carried out. From the analysis, the values of λ are computed for different values of α. The results are reported in Table 2.

Hence, it is possible to find the following boundaries for α: rigid joints with $\alpha \geq 15$, semi-rigid joints with $1.5 < \alpha < 15$ and finally, pinned joints with $\alpha \leq 1.5$.

To evaluate the coefficient β the procedure is slightly different because it is necessary to consider the nonlinearity of the material. Moreover, an initial value of α is used to compute the critical load with different values of β. In this specific case α is taken equal to 20, in order

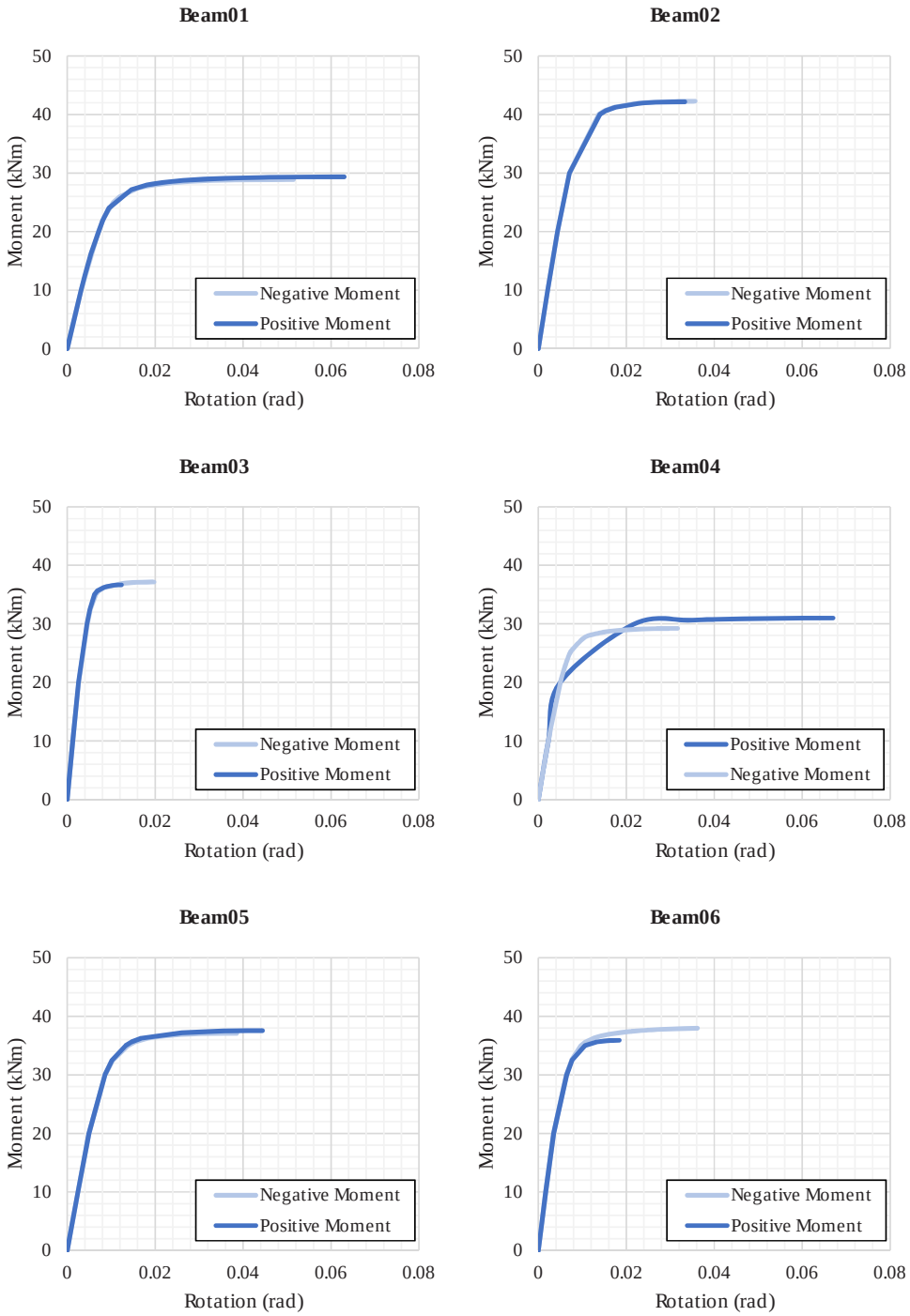

Fig. 15. Moment-rotation graphs considering a 6 mm thickness joint and moments in Y-Y direction.

to ensure the joints rigidity. Then, in order to consider different values of β, it is necessary to scale down the values of the above moment-curvature diagram with following formulas:

$$M_{pl,\beta} = \beta \cdot M_{pl}$$

$$\chi_{pl,\beta} = \beta \cdot \chi_{pl}$$

At last, applying the formula of λ, it is possible to define a graph for different values of β. λ has been computed for these values of β: Rigid, 1, 0.8, 0.5, 0.4, 0.3, 0.2, 0.1, 0.08, 0.05, 0.02, 0.01. The results are reported in Table 3.

Hence, it is possible to find the following boundaries for β: rigid joints with $\beta \geq 0.5$, semi-rigid joints with $0.08 < \beta < 0.5$, and finally, pinned joints with $\beta \leq 0.08$.

Combining the results obtained for the coefficients α and β respectively for the stiffness and the moment capacity of the joints, the joint is classified in:

- Rigid: $\alpha \geq 15$ and $\beta \geq 0.5$;
- Semi-rigid: $\alpha \geq 15$ and $0.08 < \beta < 0.5$ or $\beta \geq 0.5$ and $1.5 < \alpha < 15$;
- Pinned: $\alpha \leq 1.5$ or $\beta \leq 0.08$.

It is important to notice that joints with $\alpha \gg 15$ and $\beta \gg 0.5$ behave like joints with $\alpha = 15$ and $\beta = 0.5$, therefore this can be advantageous in a design phase (Fig. 12). In fact, using $\alpha = 15$ and $\beta = 0.5$ as design

Fig. 16. Horizontal slicing on the left and the calculated overhang support needed for fabrication (green).

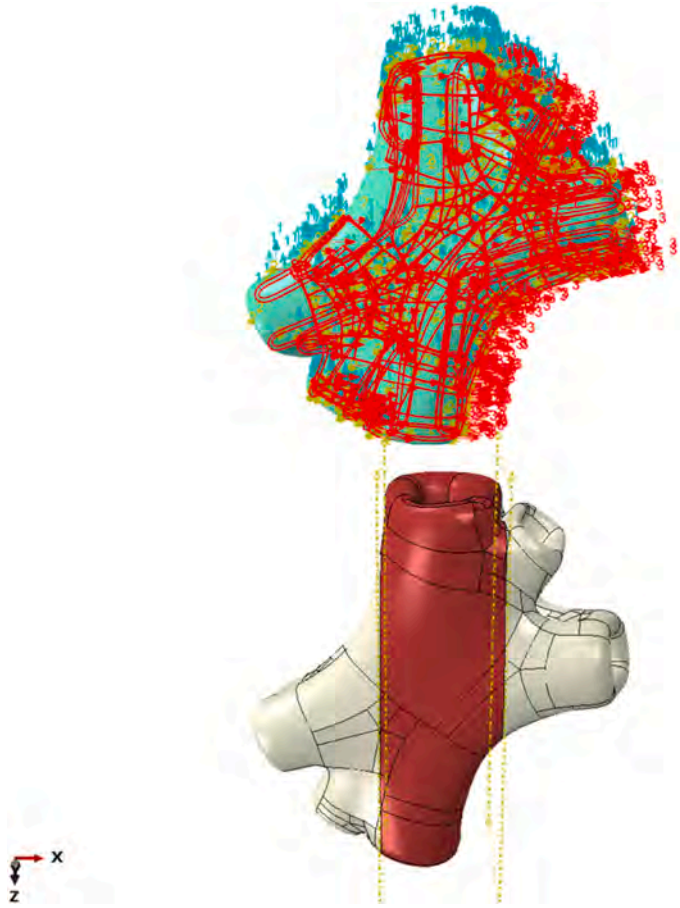

Fig. 17. Material anisotropy definition: elastic orthotropic with longitudinal direction as X (or 3) direction – up, elasto-plastic segmented orthotropic with WAAM-T in red and WAAM-D in white – down.

parameters, it is possible to design lightweight joints with a reduced quantity of material.

Once the criteria for joint classification are adapted to this case study, the behavior of this specific joint is analyzed through Finite Element Analysis (FEA). Six different directions are taken into considerations, each one along the direction of each connected member in order to define their respective partial rotational stiffness and capacity. The analyses were carried out through Abaqus software to extract the moment-rotation diagrams for each direction. The procedure is carried out by applying an increasing value of bending moment to one free end while all others are restrained (Fig. 13).

From this graph, α and β are computed easily following these steps:

The initial stiffness k of the joint along a chosen direction is calculated with this formula:

$$k = \frac{M}{\theta}$$

The coefficient α is simply the ratio between the initial stiffness k of joint and the stiffness of the adjacent beam EI/L:

$$\alpha = \frac{k}{\frac{EI}{L}}$$

The resisting bending moment of the joint $M_{pl,j,u}$ is obtained from the FEA and the resisting bending moment of the beam $M_{pl,e,u}$ is calculated with this expression:

$$M_{pl,e,u} = W_{pl} \cdot f_{yk}$$

The coefficient β is simply the ratio between the strength of the joint $M_{pl,j,u}$ and the strength of the beam $M_{pl,e,u}$:

$$\beta = \frac{M_{pl,j,u}}{M_{pl,e,u}}$$

These steps are to be repeated for all the profiles in each direction, considering both positive and negative bending moments.

Given α and β, it is possible to classify the joint as rigid, semi-rigid or pinned and hence understand its real structural behaviour. The joint is considered having a uniform thickness of 6 mm. The results are summarized in Table 4 and Fig. 14 (for X-X direction) and Table 5 and Fig. 15 (for Y-Y direction) respectively. From these results, the optimized joint must be considered as semi-rigid depending on the direction considered. Alternatively, the results of the directional classification can be used for the second iteration of the gridshell design (e.g. beam resizing) with precise formulation of rotational capacity. Alternatively, if the rigidity of the joint is preferred in the design, it is needed to return to the previous step of the workflow (post-processing of TO result) to identify WAAM-suitable alternatives that would allow for increase in the rotational stiffness or capacity. In this case, an alternative to 6-mm-shell is 12-mm-shell that ensures that the joint is fully rigid, as presented in the results below.

4.4. WAAM fabrication process

The optimized joint was finally analyzed in detail for fabrication using WAAM process. Part orientation depends on whether the focus is set on manufacturing constraints or post-processing, e.g. substrate removal. The former would in case of overhang, for example, maximize the surface area of part attached to the substrate, while the latter would minimize it. Here, the example of latter is presented.

Simple horizontal slicing (Fig. 16) results in stacking in Z-direction, thus corresponding in material orientation for orthotropic definition of

WAAM presented in Fig. 17.

Anisotropy in WAAM is mostly of orthotropic character, and as presented for stainless steel in [33], results in distinct differences in three following directions: WAAM-Longitudinal (WAAM-L), WAAM-Transversal (WAAM-T) and WAAM-Diagonal (WAAM-D). The material can then be numerically simulated through elastic engineering constants, or alternatively, through segmentation into WAAM – L/T/D, with more complex (e.g. elasto-plastic) material definition for predetermined slicing and stacking orientation, as well as for predetermined loading configuration.

The interdependency of loading configuration, part orientation, slicing and consequential material orientation in the numerical modelling exemplifies the need of using concepts, such as blended optimization when performing structural design for WAAM.

5. Conclusions

Recent architectural explorations see the application of novel computational design tools to realize complex spatial structures. These however result in difficulties when conceiving and fabricating spatial joints to connect the elements into gridshell and free forms. The opportunities of metal AM techniques, and in particular Wire-and-Arc Additive Manufacturing (WAAM) allow to apply optimization algorithms to create complex shapes with high freedom in the fabricated part, reduced construction time and almost-zero material waste.

The present work proposes a novel integrated design-for-fabrication framework based on the so-called "blended" structural optimization approach. The designs are conceived based on basic principles of conceptual structural design, manufacturing constraints proper of the selected printing process, structural requirements in terms of strengths and stiffness and topology optimization.

The approach is applied to a real case study on the re-design of complex spatial steel joints for the world's famous British Museum gridshell. A catalogue of suitable designs are generated through bi-linear structural optimization, then checked for structural requirements in terms of strengths and stiffness. The manufacturing features proper of WAAM process are embedded in the anisotropic behavior of the material, from which the most suitable printing direction is selected to optimize the joint performances. Finally, the fabrication is controlled through numerical simulations to ensure that no overhang issues are present.

The procedure is intended to simplify the application of WAAM technology in construction, while optimizing the production time and cost of joint joints for gridshells and spatial structures.

CRediT authorship contribution statement

The authors confirm contribution to the paper as follows: study conception and design: **V. Laghi**; data collection: **E. Benvenuti**; analysis and interpretation of results: **N. Babovic**; draft manuscript preparation: **V. Laghi, E. Benvenuti**; funding acquisition**: H. Kloft**. All authors reviewed the results and approved the final version of the manuscript.

Declaration of Competing Interest

The authors declare that they have no known competing financial interests or personal relationships that could have appeared to influence the work reported in this paper.

Data Availability

Data will be made available on request.

Acknowledgements

The authors gratefully acknowledge the funding by the Deutsche Forschungsgemeinschaft (DFG – German Research Foundation) – Project no. 414265976. The authors would like to thank the DFG for the support within the SFB/Transregio 277 – Additive manufacturing in construction. (Subproject A07).

Dr. Vittoria Laghi gratefully acknowledges the financial support of "Young Researchers" – Seal of Excellence 2022 grant - funded on D.M. 737/2021 resources-funded by European Union – "NextGenerationEU".

References

[1] Boje C, Guerriero A, Kubicki S, Rezgui Y. Towards a semantic construction digital twin: directions for future research. Autom Constr 2020;114:103179.
[2] Sauerwein M, Doubrovski E, Balkenende R, Bakker C. Exploring the potential of additive manufacturing for product design in a circular economy. J Clean Prod 2019;226:1138–49.
[3] A. Tedeschi, A.A.D., Algorithms-aided design: parametric strategies using Grasshopper, Le Penseur, 2014.
[4] Buchanan C, Gardner L. Metal 3D printing in construction: a review of methods, research, applications, opportunities and challenges. Eng Struct 2019;180:332–48. https://doi.org/10.1016/j.engstruct.2018.11.045.
[5] Paolini A, Kollmannsberger S, Rank E. Additive manufacturing in construction: a review on processes, applications, and digital planning methods. Addit Manuf 2019;30:100894. https://doi.org/10.1016/j.addma.2019.100894.
[6] Galjaard S, Hofman S, Ren S. New opportunities to optimize structural designs in metal by using additive manufacturing. In: Block, Knippers J, Mitra NJ, Wang W, editors. Advances in Architectural Geometry 2014. Cham: Springer International Publishing; 2015. p. 79–93.
[7] Raspall F, Banon C, Tay JC. AIRTABLE: Stainless steel printing for functional space frames. Computer-Aided Architectural Design Research in Asia (CAADRIA) 2019;1:113–22.
[8] Buchanan C, Matilainen VP, Salminen A, Gardner L. Structural performance of additive manufactured metallic material and cross-sections. J Constr Steel Res 2017;136:35–48. https://doi.org/10.1016/j.jcsr.2017.05.002.
[9] Gardner L. Metal additive manufacturing in structural engineering – review, advances, opportunities and outlook. Structures 2023;47:2178–93. https://doi.org/10.1016/J.ISTRUC.2022.12.039.
[10] Gardner L, Kyvelou P, Herbert G, Buchanan C. Testing and initial verification of the world's first metal 3D printed bridge. J Constr Steel Res 2020;172. https://doi.org/10.1016/j.jcsr.2020.106233.
[11] MX3D - Takenaka connector, (n.d.).
[12] RAMLAB, (n.d.).
[13] Snijder AH, van der Linden LPL, Goulas C, Louter C, Nijsse R. The glass swing: a vector active structure made of glass struts and 3D-printed steel joints. Glass Struct Eng 2020;5:99–116. https://doi.org/10.1007/s40940-019-00110-9.
[14] Waldschmitt B, Lange J, Costanzi CB, Knaack U, Engel T, Müller J. Robot supported wire arc additive manufacturing and milling of steel columns. Curr Perspect N Dir Mech, Model Des Struct Syst 2022:127–8. https://doi.org/10.1201/9781003348450-59.
[15] Liu J, Gaynor AT, Chen S, Kang Z, Suresh K, Takezawa A, et al. Current and future trends in topology optimization for additive manufacturing. Struct Multidiscip Optim 2018;57:2457–83. https://doi.org/10.1007/s00158-018-1994-3.
[16] Allaire G, Dapogny C, Estevez R, Faure A, Michailidis G. Structural optimization under overhang constraints imposed by additive manufacturing technologies. J Comput Phys 2017;351:295–328.
[17] Bruggi M, Laghi V, Trombetti T. Simultaneous design of the topology and the build orientation of Wire-and-Arc Additively Manufactured structural elements. Comput Struct 2021;242. https://doi.org/10.1016/j.compstruc.2020.106370.
[18] M. Bruggi, V. Laghi, T. Trombetti, Optimal design of Wire-and-Arc Additively Manufactured I-beams for prescribed deflection, Computer Assisted Methods in Engineering and Science. (2022).
[19] Adriaenssens S, Block P, Veenendaal D, Williams C. Shell structures for architecture: form finding and optimization. Routledge,; 2014.
[20] Kloft H. Logic and Form: From Isler Shells to Nonstandard Structures. J Int Assoc Shell Spat Struct 2011;169:191–9.
[21] Konstantatou M, Dall'igna M, Wilkinson S, Gallou I, Piker D. Learning lessons from Earth and Space towards Sustainable Multi-planetary Design. Spool 2021;8:39–54. https://doi.org/10.7480/spool.2021.2.5431.
[22] Castañeda E, Lauret B, Lirola JM, Ovando G. Free-form architectural envelopes: Digital processes opportunities of industrial production at a reasonable price. J Facade Des Eng 2015;3:1–13. https://doi.org/10.3233/fde-150031.
[23] Rogers A, Yoon B, Malek C. Beijing Olympic Stadium 2008 as biomimicry of a bird's nest, Architectural Structures. ARCH 2008;251.
[24] C. Yi, Re-Imagining Nature in Dense, High Rise Urban Environment: the Present and Future of Green Building Infrastructure in Singapore, (2020).
[25] Worsfold T, Bryant M, Crack J. Design of Canary Wharf Elizabeth line station and Crossrail Place oversite development. Struct Eng 2018.
[26] J. Sischka Engineering the construction of the great court roof for the British Museum Widespan Roof Struct 2000 199.
[27] S. Galjaard S. Hofman S. Ren Optim Struct Build Elem Met Using Addit Manuf 2015.
[28] Kanyilmaz A, Berto F. Robustness-oriented topology optimization for steel tubular joints mimicking bamboo structures, Material Design \& Processing. Mater Design Process Commun 2019;1:e43.

[29] Wang H, Du W, Zhao Y, Wang Y, Hao R, Yang M. Joints for treelike column structures based on generative design and additive manufacturing. J Constr Steel Res 2021;184:106794. https://doi.org/10.1016/J.JCSR.2021.106794.
[30] Laghi V, Palermo M, Gasparini G, Girelli VA, Trombetti T. On the influence of the geometrical irregularities in the mechanical response of wire-and-arc additively manufactured planar elements. J Constr Steel Res 2021;178:106490. https://doi.org/10.1016/j.jcsr.2020.106490.
[31] Huang C, Kyvelou P, Zhang R, ben Britton T, Gardner L. Mechanical testing and microstructural analysis of wire arc additively manufactured steels. Mater Des 2022;216:110544. https://doi.org/10.1016/j.matdes.2022.110544.
[32] Kyvelou P, Slack H, Daskalaki Mountanou D, Wadee MA, Britton TBen, Buchanan C, et al. Mechanical and microstructural testing of wire and arc additively manufactured sheet material. Mater Des 2020;192:108675. https://doi.org/10.1016/j.matdes.2020.108675.
[33] Laghi V, Tonelli L, Palermo M, Bruggi M, Sola R, Ceschini L, et al. Experimentally-validated orthotropic elastic model for Wire-and-Arc Additively Manufactured stainless steel. Addit Manuf 2021;42:101999. https://doi.org/10.1016/j.addma.2021.101999.
[34] Dinovitzer M, Chen X, Laliberte J, Huang X, Frei H. Effect of wire and arc additive manufacturing (WAAM) process parameters on bead geometry and microstructure. Addit Manuf 2019;26:138–46. https://doi.org/10.1016/j.addma.2018.12.013.
[35] Laghi V, Palermo M, Bruggi M, Gasparini G, Trombetti T. Blended structural optimization for wire-and-arc additively manufactured beams. Prog Addit Manuf 2022. https://doi.org/10.1007/s40964-022-00335-1.
[36] B. Standard, Eurocode 3—Design of steel structures—, BS EN 1 2006 1993-1 2005.
[37] Fan F, Ma H, Cao Z, Shen S. A new classification system for the joints used in lattice shells. Thin-Walled Struct 2011;49:1544–53. https://doi.org/10.1016/J.TWS.2011.08.002.
[38] Q. Zhou, W. Shen, J. Wang, Y.Y. Zhou, Y.M. Xie, Ameba: A new topology optimization tool for architectural design, (n.d.). ⟨https://www.ingentaconnect.com/content/iass/piass/2018/00002018/00000019/art00019#.Y_aDd-NA8oA.mendeley⟩ (accessed February 21, 2023).